materials

MDPI

Article

Synthesis and Exploration of the Lubricating Behavior of Nanoparticulated $Mo_{15}S_{19}$ in Linseed Oil

Ignacio A. Fernández-Coppel [1], Pablo Martín-Ramos [2,*], Jesús Martín-Gil [3], Ramón Pamies [4], Manuel Avella [5] and María Dolores Avilés [4]

1 Engineering of Manufacturing Processes Group, School of Industrial Engineering, University of Valladolid, C/Francisco Mendizábal 1, 47014 Valladolid, Spain; ignacio.alonso.fernandez-coppel@uva.es
2 Department of Agricultural and Environmental Sciences, EPS, Instituto de Investigación en Ciencias Ambientales de Aragón (IUCA), University of Zaragoza, Carretera de Cuarte, s/n, 22071 Huesca, Spain
3 Agriculture and Forestry Engineering Department, ETSIIAA, Universidad de Valladolid, Avenida de Madrid 44, 34004 Palencia, Spain; mgil@iaf.uva.es
4 Grupo de Ciencia de Materiales e Ingeniería Metalúrgica, Universidad Politécnica de Cartagena, Campus de la Muralla del Mar, 30202 Cartagena, Spain; ramon.pamies@upct.es (R.P.); mdolores.aviles@upct.es (M.D.A.)
5 Unidad de Microscopía Avanzada, Parque Científico UVa, Universidad de Valladolid, Paseo Belén 11, 47011 Valladolid, Spain; um.parque.cientifico@uva.es
* Correspondence: pmr@unizar.es; Tel.: +34-974-292668

Received: 11 August 2018; Accepted: 18 September 2018; Published: 19 September 2018

Abstract: Molybdenum chalcogenides present interesting properties beyond their superconducting critical temperatures and upper critical magnetic fields, making them suitable for potential applications in tribology, batteries, catalysis, or thermopower. In this study, $Mo_{15}S_{19}$ nanoparticles with an average diameter of 10 nm were synthesized via the reaction of ammonium molybdate with hydrochloric acid and elemental sulfur as reducers at 245 °C. The oxidation to MoO_3 in air was efficiently avoided by using linseed oil as a reaction medium and dispersant. Scanning electron microscopy (SEM) micrographs of the as-prepared samples revealed the presence of few-micron-size aggregates, while transmission electron microscopy (TEM) characterization evidenced that the samples were polynanocrystalline with a high degree of homogeneity in size (standard deviation of 2.7 nm). The absence of the first-order (00l) reflection in the X-ray diffraction pattern was also indicative of the absence of Mo_3S_4 stacking, suggesting that it was a non-layered material. A dispersion of the nanoparticles in linseed oil has been studied as a lubricant of steel–steel sliding contacts, showing the formation of a surface layer that reduces wear and mean friction coefficients with respect to the base oil.

Keywords: antifriction additives; linseed oil; lubricant; $Mo_{15}S_{19}$; nanoparticles

1. Introduction

$Mo_{15}S_{19}$ is a polymorph of the famous Chevrel phases [1,2]. It is a metastable binary phase that has been described as dimeric, with full formula $Mo_{30}S_{38}$ [3,4] (Figure 1).

To the best of the authors' knowledge, the direct synthesis of this phase has not been reported in the literature, including review papers [5]. The identification of $Mo_{15}S_{19}$ was reported by Tarascon and Hull [6] as a product of the oxidation of the $In_{3.3}Mo_{15}S_{19}$ phase with HCl at low temperatures. The same authors preconized for $Mo_{15}S_{19}$ the possibility to undergo topotactic redox reactions with lithium or sodium or to react at low temperatures with low melting point ternary elements to form new ternary compounds [6], in a similar fashion to its Se homologues [7,8]. Thus, the open framework structure $Mo_{15}S_{19}$ can be deemed as an interesting system for intercalation studies [5].

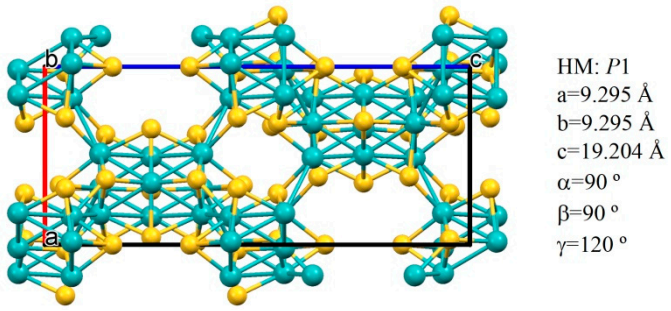

Figure 1. $Mo_{15}S_{19}$ structure, viewed along *b* axis. Plotted with Mercury [9] using the crystallographic information file (CIF) file available from the literature [3,4].

Research on these compounds, discovered over 40 years ago, initially came from their superconducting critical temperature and upper critical magnetic field [10], which opened hopes for their use in the fabrication of magnets as a replacement for the well-known Nb–Sn superconducting magnets [11]. Other fundamental features were found, such as the coexistence of magnetic order with the superconducting state. Although these features are still of interest for the scientific community, other potential applications are now foreseen, such as their use in batteries (as cathode materials), in catalysis (for the hydrodesulfurization of thiophene and/or decomposition of nitrogen oxides), and in thermopower technology (due to their low thermal conductivity and high figures of merit ZT, i.e., their ability to efficiently produce thermoelectric power) [1].

The closest Chevrel phase to $Mo_{15}S_{19}$ is $Mo_{15}S_{20}$ (or Mo_3S_4). $Mo_{15}S_{19}$ gives $Mo_{15}S_{20}$ by thermal heating at temperatures above 500 °C [12]. Mo_3S_4 crystallizes in the hexagonal space group $P6_3/m$ and consists of an equal mixture of the original Mo_9S_{27} cluster unit and the classical one $Mo_6S_8S_6$ interconnected through Mo bonds [13].

The applications of molybdenum chalcogenides as lubricant additives and surface coatings to reduce friction coefficients and surface damage and wear of materials have been extensively studied [14–17]. Although emphasis has been placed on MoS_2 polymorphs, interesting tribological properties have also been reported for other MoS_x-based coatings, such as those based on aforementioned Mo_3S_4 [18]. These materials may pose an alternative to other nanostructure lubricants [19–21], in particular to those based on graphene [22–28].

In this paper, we report a route to synthetize $Mo_{15}S_{19}$ using linseed oil as a reaction medium and dispersant, with a view of obtaining a non-oxidized nano-particulated material. The friction and wear reducing ability of a dispersion of the nanoparticles in the environmentally-friendly vegetable linseed oil (one of the natural oils suggested to replace mineral oil in, for instance, drilling fluids [29]) has been assessed.

2. Materials and Methods

2.1. Materials

Ammonium molybdate tetrahydrate ($(NH_4)_6Mo_7O_{24}\cdot 4H_2O$; CAS No. 12054-85-2; purity ≥99%) was purchased from Sigma-Aldrich Química S.L. (Madrid, Spain). Linseed oil was purchased as NaturGreen line oil from Laboratorios Almond S.L. (Murcia, Spain). Hydrochloric acid, sulfur, and hexane were commercially available analytical-grade products. All chemicals used in the experiment were used without further purification.

2.2. Synthesis

$Mo_{15}S_{19}$ nanoparticles were synthesized via the reaction of ammonium molybdate with hydrochloric acid and elemental sulfur as reducing agents, in linseed oil as the reaction medium. A total of 1.23 g of $(NH_4)_6Mo_7O_{24}\cdot 4H_2O$ (1 mmol) was stirred in 27 mL linseed oil, proceeding with the stirring of the mixture while 2 mL of hydrochloric acid fuming 37% was carefully added dropwise.

Upon reaction, blue and green colors appeared. Subsequently, 0.256 g of sulfur powder S_8 (1 mmol) was added and a change in color to red occurred. The system was heated under stirring at 245 °C for 100 min until a black color appeared. Aliquots were taken from the reaction flask and were allowed to cool down to room temperature, and the resulting nano-$Mo_{15}S_{19}$ was then collected by centrifugation by adding excess hexane–methanol–water (1:1:1) three times. The as-prepared $Mo_{15}S_{19}$ (slightly soaked in linseed oil) was a stable product and the corrosive effects of chloride remained minimized by the use of hexane–hydromethanol as the washing liquid.

For tribological tests, and to avoid the potential corrosive effects of halides on metals, an entirely chloride-free lubricant may be obtained by sonication of 100 mL of a 0.0195 M solution of $Mo_{15}S_{19}$ nanoparticles in linseed oil (prepared according the previous procedure) for five periods of 5 min each at 60 °C, using 20 mL of a methanol/water mixture (1:1, v/v) each time.

A probe-type UIP1000hdT ultrasonicator (Hielscher, Teltow, Germany; 1000 W, 20 kHz) was used for the sonication of solutions.

2.3. Characterization

The as-prepared $Mo_{15}S_{19}$ was characterized by Fourier-transform infrared spectroscopy (FTIR), scanning electron microscopy (SEM), transmission electron microscopy (TEM), and X-ray powder diffraction (XRPD).

The vibrational spectrum in the 400–4000 cm^{-1} spectral range was characterized using a Thermo Scientific (Waltham, MA, USA) Nicolet iS50 FT-IR Spectrometer, equipped with an in-built diamond attenuated total reflection (ATR) system, with a 1 cm^{-1} spectral resolution and 64 scans.

X-ray powder diffraction patterns were obtained using a Bruker (Billerica, MA, USA) Discover D8 powder diffractometer in a Bragg–Brentano geometry.

Scanning electron microscopy (SEM) and transmission electron microscopy (TEM) images were collected with an FEI (Hillsboro, OR, USA) Quanta 200FEG microscope and with a JEOL (Akishima, Tokyo, Japan) JEM-FS2200 HRP microscope, respectively.

2.4. Rheological and Tribological Study

Viscosity measurements of the base linseed oil and of the dispersion of nanoparticles in linseed oil were performed with an AR-G2 rotational rheometer (TA instruments; New Castle, DE, USA), using a plate-on-plate configuration. The shear flow influence on the viscosity was determined at 25 °C by changing the shear rate from 10^{-2} to 500 s^{-1}. The influence of temperature on viscosity was studied from 25 °C to 100 °C under a constant shear rate of 50 s^{-1}.

Tribological tests according to ASTM G-99 standard were carried out in a pin-on-disk ISC 200PC tribometer (Implant Science Co; Wakefield, MA, USA) under ambient conditions (22 ± 1 °C; RH: 50–55%). The materials used in the tribological tests were stainless steel balls (nominal composition in weight percentage: <0.03 C; 16−18.5 Cr; 10−14 Ni; 2−3 Mo; <2 Mn; <1 Si; <0.045 P; <0.03 S; balance Fe; hardness: 195 HV) with 1.5 mm sphere radius and AISI 316L stainless steel disks (25 mm diameter; 2.5 mm thickness; surface roughness Ra 0.12−0.13 μm). The disk surface was completely covered with the lubricant before applying a normal load of 0.49 N, at a speed of 0.1 $m{\cdot}s^{-1}$ (sliding radius 9 mm), for a sliding distance of 372 m (sliding time: 1 h). The materials were washed with *n*-hexane and dried in air, before and after each test. Wear tracks sections and surface topography were determined with a Talysurf CLI 3D optical profiler (AMETEK; Berwyn, PA, USA). Friction coefficients in each test were calculated as average values from the entire duration of the test. Final friction coefficients and wear rates were calculated as mean values after at least three tests under the same conditions. The cross sectional profiles of the wear tracks were obtained from an average of 300 profiles, each of which consisted of 300 points.

3. Results and Discussion

3.1. Vibrational Characterization

ATR-FTIR spectra were acquired to investigate the $Mo_{15}S_{19}$–linseed oil interaction. In the spectra depicted in Figure 2, absorption bands characteristic of linseed oil [30] appeared at 2923 cm^{-1} (H-C-H asymmetric) and 2853 cm^{-1} (H-C-H symmetric); 3010 cm^{-1} (C=C-H asymmetric stretching); 1742 cm^{-1} (C=O stretching); 1459–1456 cm^{-1} (asymmetric CH_3 bending); 1240, 1164, and 1095 cm^{-1} (characteristic triglyceride ester triplet); and 720 cm^{-1} ($(CH_2)_n$ rocking/cis-(C-H)=CH wagging).

$Mo_{15}S_{19}$ characteristic bands appear at 579–586 cm^{-1} (ν(S-S) stretching mode, suggesting some double-bond character); 528 cm^{-1} (also attributed to ν(S-S) stretching modes); and 464 cm^{-1} (assigned to ν(Mo-S) stretching) [31].

No appreciable interactions were evidenced between linseed oil and $Mo_{15}S_{19}$ from the vibrational spectra, although some shifts could be observed for three (weak) linseed oil bands: 16 cm^{-1} for the $\omega(CH_2)$ band at 1376 cm^{-1} (vs. 1360 cm^{-1} in the spectrum of the mixture), 19 cm^{-1} for the band at 1237 cm^{-1} associated with ν(C-O) in triglycerides ester linkage (vs. 1218 cm^{-1} in the spectrum of the mixture), and 19 cm^{-1} for the band at 1068 cm^{-1} related to ν(C-O-C) ethers (vs. 1049 cm^{-1} for the mixture) [32].

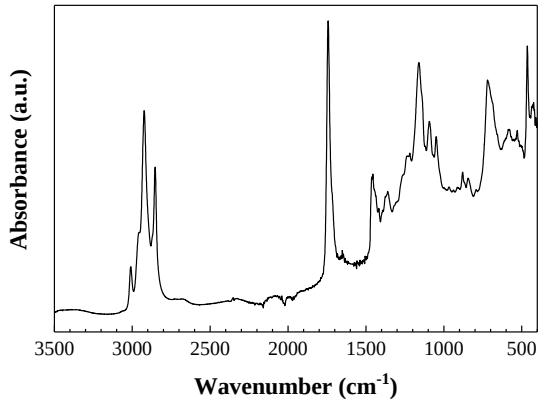

Figure 2. Attenuated total reflection (ATR)-Fourier-transform infrared spectroscopy (FTIR) spectra of $Mo_{15}S_{19}$ nanoparticles dispersion in linseed oil.

3.2. X-ray Powder Diffraction Analysis

The intensity peaks at 11.04, 12.5, 14.3, 43.04, and 45.4° can be ascribed to hexagonal $Mo_{15}S_{19}$ (JCPDS card # 40-0936) in good agreement with the calculated pattern (Figure 3).

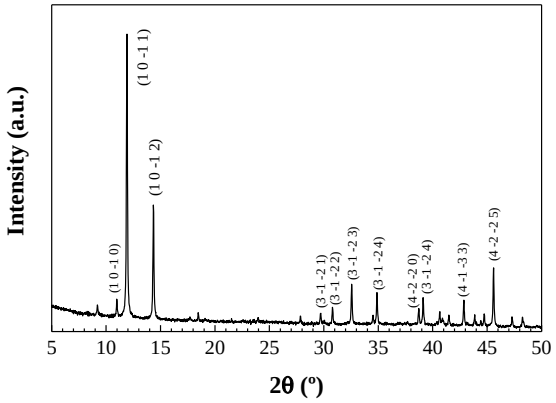

Figure 3. Experimental X-ray powder diffraction patterns for $Mo_{15}S_{19}$ nanoparticles. Four-index notation of the Miller indices has been used to allow direct comparison with the diffractograms reported in the literature [3,4].

3.3. SEM Analysis

The morphology analysis of the synthesized $Mo_{15}S_{19}$ revealed the presence of few-micron-size aggregates, such as the one depicted in Figure 4. These would result from the tendency of unmodified nanoparticles to settle down after a finite time if the oil is kept stationary, a behavior that can be minimized by using surfactant-modified nanoparticles [33].

As the magnification in the SEM was insufficient to clearly show the nano-particulate nature of the material, samples were sonicated and subjected to TEM analysis. The sonication of oil dispersions has been reported to significantly improve the dispersion quality compared with mechanical shaking and stirring, although it would not completely disaggregate nanoparticles, according to Mosleh, et al. [34].

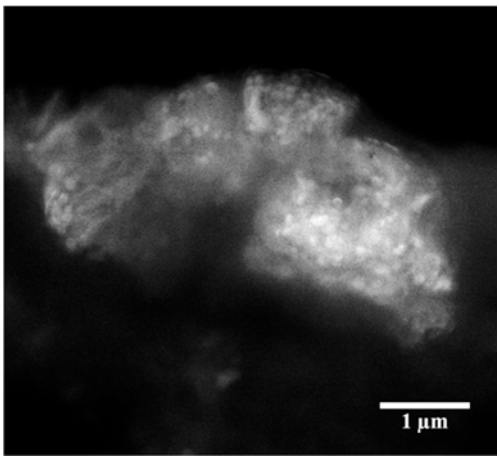

Figure 4. Scanning electron microscopy (SEM) micrograph of as-prepared $Mo_{15}S_{19}$ particles showing their aggregation state prior to sonication.

3.4. SAED Pattern and TEM Images

The selected area electron diffraction (SAED) pattern (inset in Figure 5a), compatible either with nanoparticles of single-crystalline structure or with a poly-nanocrystalline sample, was not conclusive. Close inspection of TEM images of as-prepared $Mo_{15}S_{19}$ particles dispersed in methanol (Figure 5a–c) evidenced their nanoscale size, with an average diameter of 10 nm (standard deviation of 2.7 nm, Figure 5d), smaller than the 70 nm diameter reported in Rosentsveig, et al. [35]; than the 50 nm diameter reported in Santillo, et al. [36]; and than the 10–30 nm diameters found by Duphil, et al. [37] for MoS_2. Only in the work by Yu, et al. [38], smaller diameters (5 nm) were attained. However, it is worth noting that, according to Kogovšek and Kalin [39], the NPs size and morphology would not significantly affect the coefficient of friction, which would mostly depend on the NPs' material.

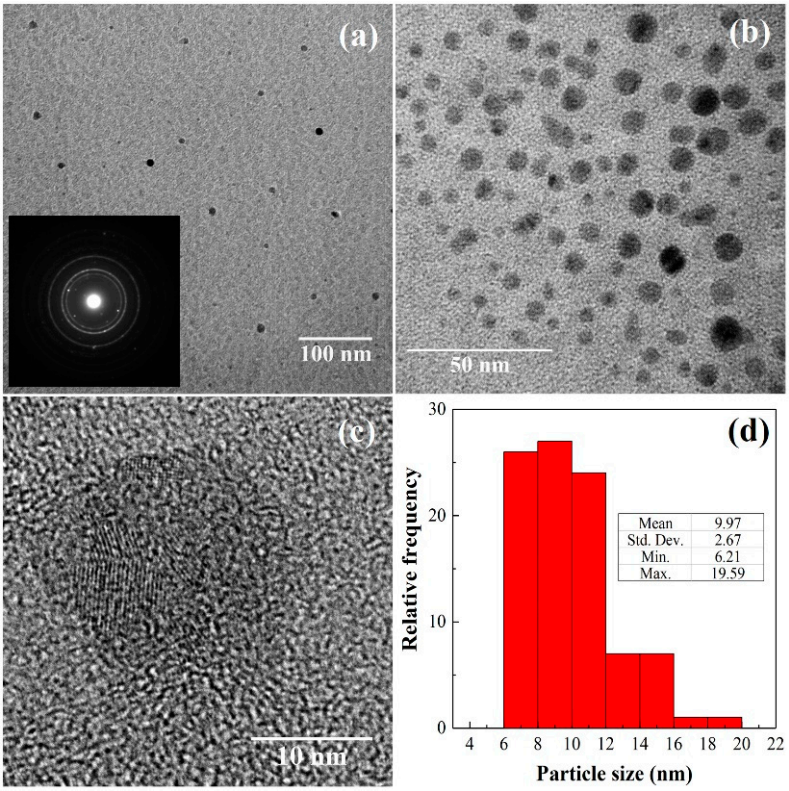

Figure 5. (**a**–**c**) Transmission electron microscopy (TEM) micrographs of $Mo_{15}S_{19}$ prepared in linseed oil at different magnifications. The inset in (**a**) shows the selected area electron diffraction (SAED) pattern. (**d**) Histogram showing the particle size distribution.

3.5. Rheological Study

The variation of the viscosity of the base linseed oil and of the dispersion of $Mo_{15}S_{19}$ in the base oil with increasing temperature under constant shear rate (50 s^{-1}) and with increasing shear rate under constant temperature (25 °C) are shown in Figure 6. In both samples, there was an expected decrease of the viscosity with the increasing values of temperature. The dispersion showed higher viscosity values than those of the base oil, because of the presence of particles in the fluid, which would act as obstacles, and thus the fluid presented a higher resistance to flow. Only at 100 °C, the viscosity values of both fluids became similar. While the base oil showed a Newtonian behavior, the dispersion showed a slight decrease of its viscosity over the whole range of shear rate investigated. This shear thinning effect can be attributed to the disruption of agglomerates [40].

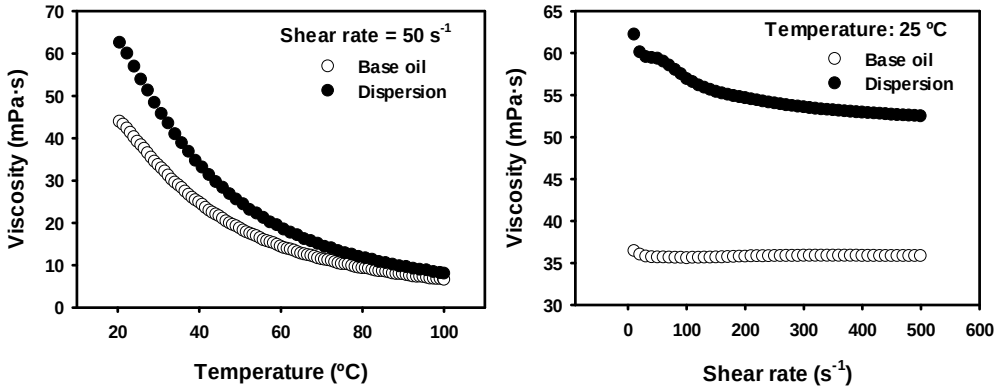

Figure 6. Viscosity variation with temperature and with shear rate for both lubricants.

3.6. Tribological Study

As shown in Table 1, the dispersion was able to reduce the friction coefficient by 23.4% with respect to the base oil. In each test, the friction coefficient was calculated as an average of all the friction values recorded from the entire test duration.

Table 1. Average values and standard deviations (in brackets) of the coefficient of friction across three tests.

Lubricant: Base Oil	**Coefficient of Friction**
Test 1	0.097 (±0.004)
Test 2	0.115 (±0.007)
Test 3	0.109 (±0.003)
Average	**0.107 (±0.009)**
Lubricant: Dispersion	**Coefficient of Friction**
Test 1	0.081 (±0.015)
Test 2	0.079 (±0.013)
Test 3	0.085 (±0.010)
Average	**0.082 (±0.003)**

Figure 7 shows the evolution of the coefficient of friction (μ) with sliding distance for both lubricants. While the neat base oil (Figure 7, black) showed a constant friction value, the dispersion was able to reduce friction values during 300 m, to reach a final friction value similar to that of the base oil (Figure 7, red). This result could be related with the stability of the dispersion and with the increasing values of viscosity when nanoparticles are added, as shown in Figure 6. The formation of agglomerates and the deposition of the nanoparticles on the sliding surfaces could account for the final friction increase.

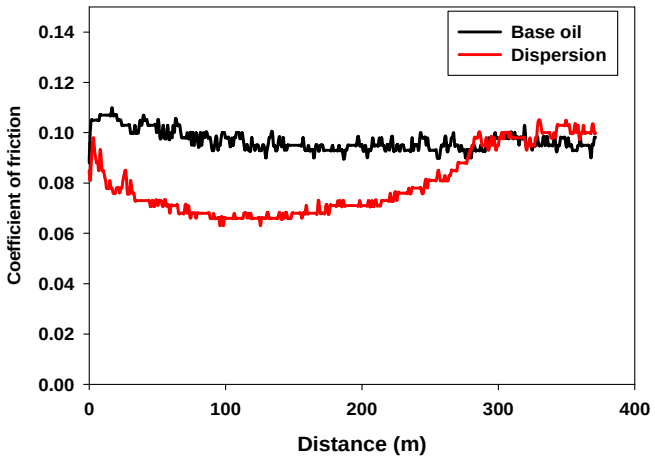

Figure 7. Variation of coefficient of friction (COF) with sliding distance for the base oil (*black*) and the dispersion (*red*).

Regarding the behavior of the base oil, from an analysis of the scoring resistance of oils according to the welding load and load wear index, Grigoriev, et al. [41] showed that, according to GOST9490-75, linseed oil featured better tribotechnical properties than those of I20A industrial basic oil. They concluded that it was most likely that the observed advantage of linseed oil was related to the high content of linolenic acid triglycerides, which is intrinsic for a relatively large number of unsaturated bonds, in contrast with, for instance, coconut oil (assayed as a nanolubricant with MoS_2 nanoparticles by Koshy, Rajendrakumar and Thottackkad [33]).

The μ value for the dispersion was similar to that obtained for acrylated epoxidized linseed oil (AELO) based bio-nanocomposites with low TiO_2 content (1 wt.%) [42]. It is also worth noting that the final value was comparable to the best value reported for linseed oil bonded to mercaptosilane treated aluminum [43]. Nonetheless, it should be noted that because the tribological tests in these two studies were performed under different operating parameters as in the present study, comparisons of the coefficients of friction above should be taken with caution.

The tribological performance of the $Mo_{15}S_{19}$–linseed oil dispersion may be explained by taking an alternative view of it as a nanocomposite fluid based on the vegetable oil with $Mo_{15}S_{19}$ as a nano-reinforcement, in a similar way to the aforementioned linseed oil–TiO_2 green nanocomposites reported by Díez-Pascual and Díez-Vicente [42], for which strong reductions in the coefficient of friction and the wear rate were attained with the highest TiO_2 content. In both cases, the dispersed inorganic particles would reduce the free volume and the mobility of the oil polymer chains, leading to more compact networks. As in the case of linseed oil–TiO_2, the presumably high thermal conductivity of $Mo_{15}S_{19}$ would enable a rapid heat dissipation, hence resulting in a lower temperature in the sliding contact.

3.7. Surface Analysis and Wear Mechanisms

Figure 8a shows an SEM micrograph of the wear track on the surface of the AISI 316L stainless steel disk after lubrication with the base oil, while Figure 8b depicts the results of the energy dispersive x-ray spectrometry (EDX) analysis of the selected area, showing the composition of the stainless steel. The severe wear was the result of plastic deformation, as may be observed on the edges of the wear track, and the result of abrasion, as evidenced by the parallel abrasion grooves along the wear track, parallel to the sliding direction.

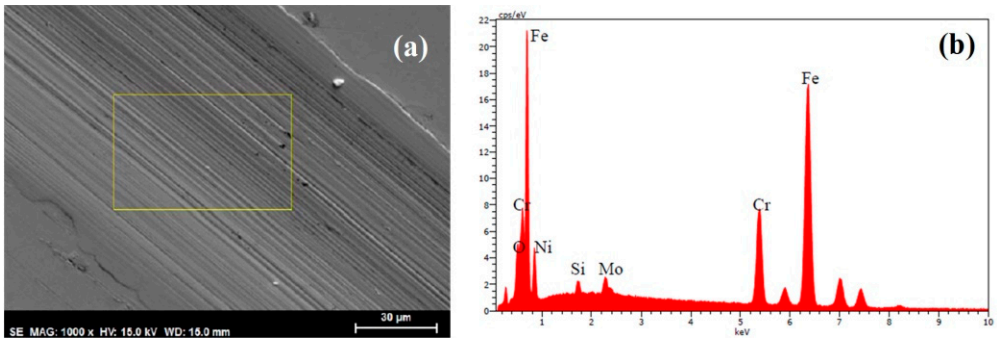

Figure 8. (**a**) SEM micrograph of the wear track on AISI 316L stainless steel disk after lubrication with base oil at 1000× magnification and (**b**) EDX spectrum of the selected area.

The severity of the surface damage was shown by the surface topography profilometry image of a 3 mm × 2 mm section of the wear track, in which the origin was set on the highest value (Figure 9a). The cross sectional profile of the wear track is shown in Figure 9b. The average total wear volume after three tests was 1.23×10^{-3} mm^3 (standard deviation 7.7×10^{-4}).

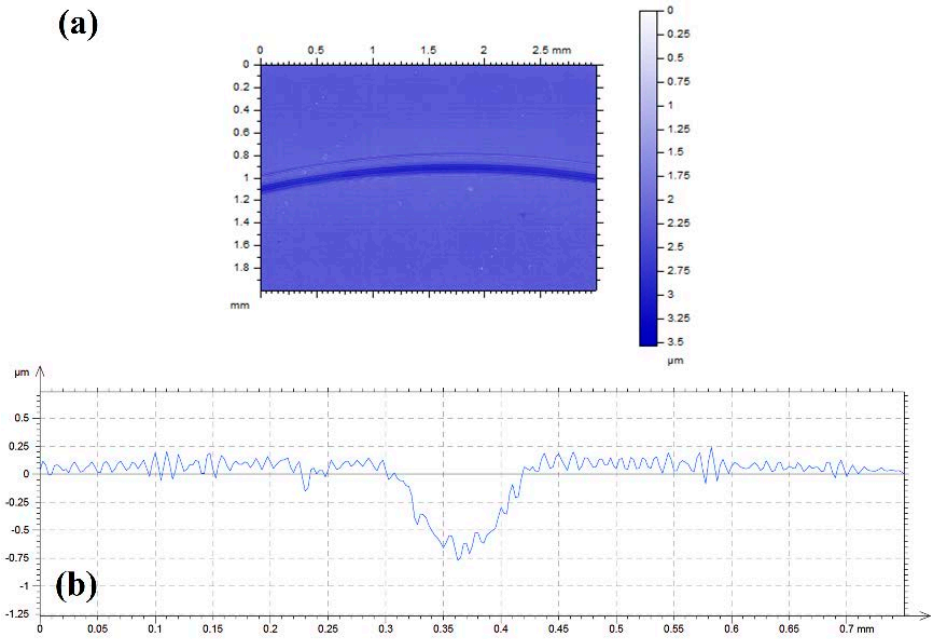

Figure 9. (**a**) Surface topography and (**b**) cross sectional profile of the wear track on AISI 316L disk after lubrication with base oil.

In Figure 10a, the SEM micrograph of the wear track on the steel surface after lubrication with the dispersion is shown. Analogously to the wear track seen after lubrication with the base oil in absence of nanoparticles, the presence of edges and parallel abrasion grooves along the track evidenced a similar, but significantly less pronounced, plastic deformation due to abrasion. Interestingly, the iron and molybdenum and/or sulphur element maps (Figure 10b) showed that a Mo and S rich layer covered the surface outside the wear track, with some particles inside the wear path. The presence of nanoparticles on the wear path may point to two mechanisms of reducing asperity contact: by filling the valleys of contacting surfaces and by the easy shearing of trapped solid lubricant nanoparticles at the interface without the formation of an adhered film [34,44].

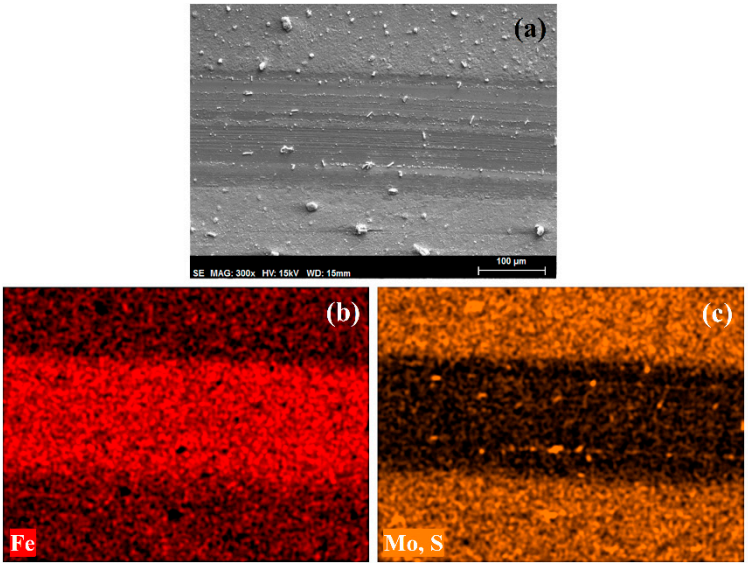

Figure 10. (**a**) SEM micrograph and (**b**,**c**) element maps of the wear track on AISI 316L disk after lubrication with the dispersion of $Mo_{15}S_{19}$ nanoparticles in linseed oil.

The surface topography (Figure 11a) showed very mild surface damage. In fact, the cross sectional profile (Figure 11b) did not show any material loss, as the surface profile was very similar inside and outside the wear path (notice the nanometer scale). The removed wear volume could not be reliably determined, making it impossible to compare the improvement in the normalized wear coefficients with those reported in the studies by Tomala, et al. [45] and Paskvale, et al. [46] on MoS_2 nanotubes in other oils.

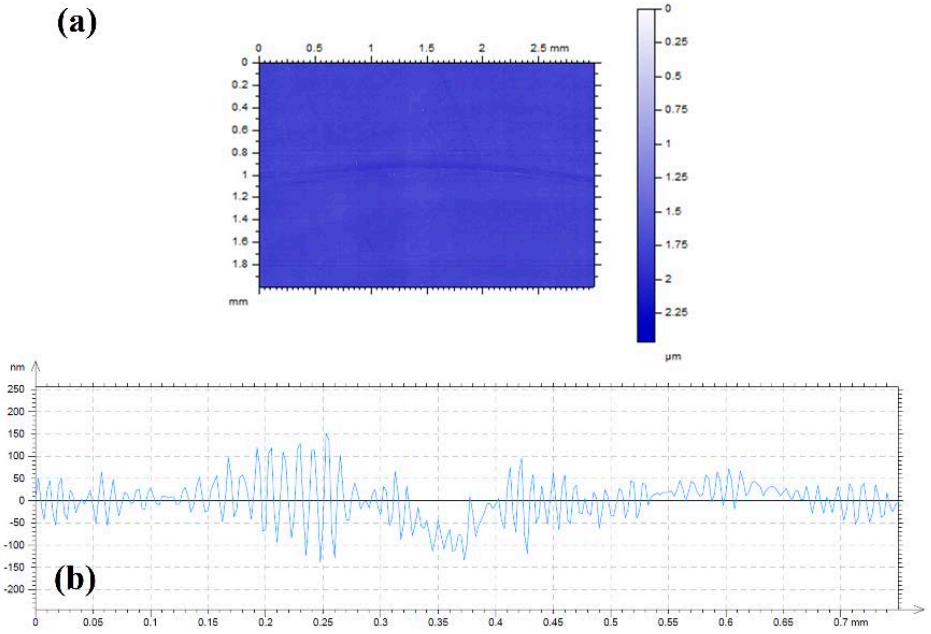

Figure 11. (**a**) Surface topography and (**b**) cross sectional profile of the wear track on AISI 316L disk after lubrication with the dispersion of nanoparticles in linseed oil.

Stainless steel balls also showed wear scars at the end of the tests (Figure 12). In agreement with the different wear mechanisms described for steel disks, the wear scar on the ball after lubrication with base oil showed abrasive wear (Figure 12a), while a smooth circular scar—free from adhered material—was observed after lubrication with the dispersion (Figure 12b).

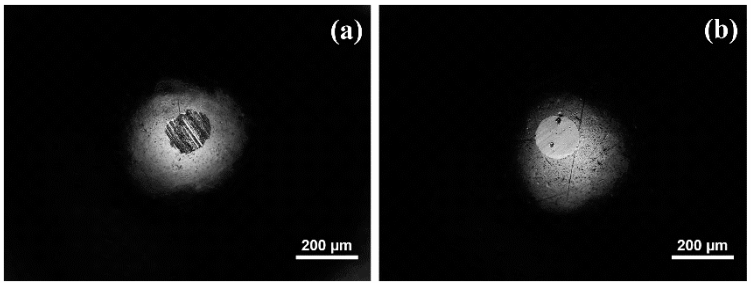

Figure 12. Wear scars on AISI 316L balls: (**a**) lubricated with base oil; (**b**) lubricated with the dispersion.

4. Conclusions

A soft chemical route to synthetize $Mo_{15}S_{19}$ using linseed oil as the reaction medium was presented, which yielded a non-oxidized nano-particulated material. The resulting $Mo_{15}S_{19}$ nanoparticles featured a regular size (with an average diameter of 10 nm) and some aggregation degree, while oxidation to MoO_3 in air was efficiently avoided by linseed oil dispersant. With a view to assess their applicability as a lubricant additive and/or surface coating, rheological and tribological studies were conducted for a dispersion of the nanoparticles in linseed oil. The dispersion showed higher viscosity values than those of the base oil, and was found to reduce the friction coefficient by

23% with respect to the base oil. While the base oil displayed a Newtonian behavior, the dispersion presented a mild shear thinning effect probably because of the fraction of aggregates observed in SEM. The friction reduction lasted for only 300 m, and afterwards, the coefficient of friction increased to the value of the base oil. Tribological test results showed that the dispersion formed a surface layer that protected stainless steel surface against wear. The higher viscosity of the dispersion with respect to the base oil could account for its higher ability to support the applied load and to separate more effectively the sliding surfaces. This factor, together with the deposition of a layer of particles from the dispersion on the steel surface, would be responsible for the noticeable wear reduction observed. Further research to optimize the $Mo_{15}S_{19}$ loading, and to prevent the formation of agglomerates and the deposition of the nanoparticles on the sliding surfaces, is underway.

Author Contributions: Conceptualization, I.A.F.-C., P.M.-R., and J.M.-G.; Formal analysis, I.A.F.-C., P.M.-R., R.P., and M.D.A.; Funding acquisition, R.P.; Investigation, P.M.-R., J.M.-G., R.P., M.A., and M.D.A.; Methodology, I.A.F.-C., J.M.-G., and R.P.; Resources, J.M.-G. and R.P.; Supervision, J.M.-G. and R.P.; Validation, I.A.F.-C., P.M.-R., J.M.-G., and R.P.; Visualization, P.M.-R. and M.D.A.; Writing—original draft, P.M.-R., J.M.-G., and M.D.A.; Writing—review & editing, P.M.-R., R.P., and M.A.

Funding: P.M.-R. acknowledges the financial support of Santander Universidades through "Becas Iberoamérica. Santander Investigación—Santander Universidades" program. R.P. and M.D.A. acknowledge Ministerio de Economía, Industria y Competitividad (MINECO, Spain), EU FEDER Program (Grants # MAT2014-55384-P and # MAT2017-85130-P), and Fundación Séneca Agencia de Ciencia y Tecnología de la Región de Murcia "Ayuda a las Unidades y Grupos de Excelencia Científica de la Región de Murcia (Programa Séneca 2014)" (Grant # 19877/GERM/15) for financial support. M.D. Avilés acknowledges a research fellowship (Grant # BES-2015-074836) to MINECO.

Acknowledgments: Access to TAIL-UC facility funded under QREN-Mais Centro project ICT-2009-02-012-1980 is gratefully acknowledged.

Conflicts of Interest: The authors declare no conflict of interest. The funders had no role in the design of the study; in the collection, analyses, or interpretation of data; in the writing of the manuscript, and in the decision to publish the results.

References

1. Peña, O. Chevrel phases: Past, present and future. *Phys. C Supercond. Appl.* **2015**, *514*, 95–112. [CrossRef]
2. Chevrel, R.; Hirrien, M.; Sergent, M. Superconducting Chevrel phases: Prospects and perspectives. *Polyhedron* **1986**, *5*, 87–94. [CrossRef]
3. Jain, A.; Ong, S.P.; Hautier, G.; Chen, W.; Richards, W.D.; Dacek, S.; Cholia, S.; Gunter, D.; Skinner, D.; Ceder, G.; et al. Commentary: The Materials Project: A materials genome approach to accelerating materials innovation. *APL Mater.* **2013**, *1*, 011002. [CrossRef]
4. Persson, K. Materials Data on $Mo_{15}S_{19}$ (SG: 176) by Materials Project. Available online: https://materialsproject.org/materials/mp-31257/ (accessed on 7 July 2018).
5. Afanasiev, P. Synthetic approaches to the molybdenum sulfide materials. *C. R. Chim.* **2008**, *11*, 159–182. [CrossRef]
6. Tarascon, J.M.; Hull, G.W. On several new ternary molybdenum sulfide phases $M_{3.4}Mo_{15}S_{19}$ (M = vacancy, Li, Na, K, Zn, Cd, Sn and Tl). *Mater. Res. Bull.* **1986**, *21*, 859–869. [CrossRef]
7. Tarascon, J. Electrochemical insertion of lithium and sodium in the two crystallographic forms of a new molybdenum chalcogenide phase $Mo_{15}Se_{19}$. *Solid State Ionics* **1986**, *18–19*, 768–772. [CrossRef]
8. Tarascon, J.M.; Hull, G.W.; Waszczak, J.V. Synthesis, structural and physical properties of the binary molybdenum chalcogenide phase $Mo_{15}Se_{19}$ and of the related compounds $M_2Mo_{15}Se_{19}$ and $M_3Mo_{15}Se_{19}$ (M=group 1A metal; Sn,Pb;Cd). *Mater. Res. Bull.* **1985**, *20*, 935–946. [CrossRef]
9. Macrae, C.F.; Edgington, P.R.; McCabe, P.; Pidcock, E.; Shields, G.P.; Taylor, R.; Towler, M.; van de Streek, J. Mercury: Visualization and analysis of crystal structures. *J. Appl. Crystallogr.* **2006**, *39*, 453–457. [CrossRef]
10. Chevrel, R.; Sergent, M. Chemistry and structure of ternary molybdenum chalcogenides. In *Superconductivity in Ternary Compounds I*; Fischer, Ø., Maple, M.B., Eds.; Springer: Berlin/Heidelberg, Germany, 1982; Volume 32, pp. 25–86.
11. Ramsbottom, H.D.; Hampshire, D.P. Improved critical current density and irreversibility line in HIP'ed Chevrel phase superconductor $PbMo_6S_8$. *Phys. C Supercond.* **1997**, *274*, 295–303. [CrossRef]

12. Salloum, D.; Gautier, R.; Potel, M.; Gougeon, P. $Mo_{15}S_{20}$: First evidence of a new molybdenum cluster type in a metastable solid-state compound. *Chem. Eur. J.* **2006**, *12*, 8513–8517. [CrossRef] [PubMed]
13. Fukuoka, H.; Masuoka, K.; Hanaoka, T.; Inumaru, K. New polymorph of Mo_3S_4 prepared using a high-pressure synthesis technique: Crystal structure, electronic property, and band calculation. *Inorg. Chem.* **2013**, *52*, 7918–7922. [CrossRef] [PubMed]
14. Al-Jeboori, Y.; Kosarieh, S.; Morina, A.; Neville, A. Investigation of pure sliding and sliding/rolling contacts in a DLC/Cast iron system when lubricated in oils containing MoDTC-Type friction modifier. *Tribol. Int.* **2018**, *122*, 23–37. [CrossRef]
15. Parenago, O.P.; Kuz'mina, G.N.; Zaimovskaya, T.A. Sulfur-containing molybdenum compounds as high-performance lubricant additives (Review). *Pet. Chem.* **2017**, *57*, 631–642. [CrossRef]
16. Tang, Z.; Li, S. A review of recent developments of friction modifiers for liquid lubricants (2007–present). *Curr. Opin. Solid State Mater. Sci.* **2014**, *18*, 119–139. [CrossRef]
17. Theerthagiri, J.; Senthil, R.A.; Senthilkumar, B.; Reddy Polu, A.; Madhavan, J.; Ashokkumar, M. Recent advances in MoS_2 nanostructured materials for energy and environmental applications—A review. *J. Solid State Chem.* **2017**, *252*, 43–71. [CrossRef]
18. Ilie, F.I.; Tita, C.M. Tribological properties of solid lubricant nanocomposite coatings obtained by magnetron sputtered of MoS_2/metal (Ti, Mo) nanoparticles. *Proc. Rom. Acad. Ser. A Math. Phys. Tech. Sci. Inf. Sci.* **2007**, *8*, 1–5.
19. Gulzar, M.; Masjuki, H.H.; Kalam, M.A.; Varman, M.; Zulkifli, N.W.M.; Mufti, R.A.; Zahid, R. Tribological performance of nanoparticles as lubricating oil additives. *J. Nanopart. Res.* **2016**, *18*, 223. [CrossRef]
20. Shahnazar, S.; Bagheri, S.; Abd Hamid, S.B. Enhancing lubricant properties by nanoparticle additives. *Int. J. Hydrog. Energy* **2016**, *41*, 3153–3170. [CrossRef]
21. Xiao, H.; Liu, S. 2D nanomaterials as lubricant additive: A review. *Mater. Des.* **2017**, *135*, 319–332. [CrossRef]
22. Rasheed, A.K.; Khalid, M.; Rashmi, W.; Gupta, T.C.S.M.; Chan, A. Graphene based nanofluids and nanolubricants—Review of recent developments. *Renew. Sustain. Energy Rev.* **2016**, *63*, 346–362. [CrossRef]
23. Cheng, Z.-L.; Qin, X.-X. Study on friction performance of graphene-based semi-solid grease. *Chin. Chem. Lett.* **2014**, *25*, 1305–1307. [CrossRef]
24. Mura, A.; Curà, F.; Adamo, F. Evaluation of graphene grease compound as lubricant for spline couplings. *Tribol. Int.* **2018**, *117*, 162–167. [CrossRef]
25. Fan, X.; Wang, L. High-performance lubricant additives based on modified graphene oxide by ionic liquids. *J. Colloid Interface Sci.* **2015**, *452*, 98–108. [CrossRef] [PubMed]
26. Kamel, B.M.; Mohamed, A.; El Sherbiny, M.; Abed, K.A.; Abd-Rabou, M. Tribological properties of graphene nanosheets as an additive in calcium grease. *J. Dispers. Sci. Technol.* **2016**, *38*, 1495–1500. [CrossRef]
27. Dou, X.; Koltonow, A.R.; He, X.; Jang, H.D.; Wang, Q.; Chung, Y.-W.; Huang, J. Self-dispersed crumpled graphene balls in oil for friction and wear reduction. *Proc. Natl. Acad. Sci. USA* **2016**, *113*, 1528–1533. [CrossRef] [PubMed]
28. Huang, H.D.; Tu, J.P.; Gan, L.P.; Li, C.Z. An investigation on tribological properties of graphite nanosheets as oil additive. *Wear* **2006**, *261*, 140–144. [CrossRef]
29. Kania, D.; Yunus, R.; Omar, R.; Abdul Rashid, S.; Mohamad Jan, B. A review of biolubricants in drilling fluids: Recent research, performance, and applications. *J. Pet. Sci. Eng.* **2015**, *135*, 177–184. [CrossRef]
30. Vahur, S.; Teearu, A.; Peets, P.; Joosu, L.; Leito, I. ATR-FT-IR spectral collection of conservation materials in the extended region of 4000-80 cm^{-1}. *Anal. Bioanal. Chem.* **2016**, *408*, 3373–3379. [CrossRef] [PubMed]
31. Weber, T.; Muijsers, J.C.; van Wolput, J.H.M.C.; Verhagen, C.P.J.; Niemantsverdriet, J.W. Basic reaction steps in the sulfidation of crystalline MoO_3 to MoS_2, as studied by X-ray photoelectron and infrared emission spectroscopy. *J. Phys. Chem.* **1996**, *100*, 14144–14150. [CrossRef]
32. De Viguerie, L.; Payard, P.A.; Portero, E.; Walter, P.; Cotte, M. The drying of linseed oil investigated by Fourier transform infrared spectroscopy: Historical recipes and influence of lead compounds. *Prog. Org. Coat.* **2016**, *93*, 46–60. [CrossRef]
33. Koshy, C.P.; Rajendrakumar, P.K.; Thottackkad, M.V. Evaluation of the tribological and thermo-physical properties of coconut oil added with MoS_2 nanoparticles at elevated temperatures. *Wear* **2015**, *330–331*, 288–308. [CrossRef]
34. Mosleh, M.; Atnafu, N.D.; Belk, J.H.; Nobles, O.M. Modification of sheet metal forming fluids with dispersed nanoparticles for improved lubrication. *Wear* **2009**, *267*, 1220–1225. [CrossRef]

35. Rosentsveig, R.; Gorodnev, A.; Feuerstein, N.; Friedman, H.; Zak, A.; Fleischer, N.; Tannous, J.; Dassenoy, F.; Tenne, R. Fullerene-like MoS_2 nanoparticles and their tribological behavior. *Tribol. Lett.* **2009**, *36*, 175–182. [CrossRef]
36. Santillo, G.; Deorsola, F.A.; Bensaid, S.; Russo, N.; Fino, D. MoS_2 nanoparticle precipitation in turbulent micromixers. *Chem. Eng. J.* **2012**, *207–208*, 322–328. [CrossRef]
37. Duphil, D.; Bastide, S.; Lévy-Clément, C. Chemical synthesis of molybdenum disulfide nanoparticles in an organic solution. *J. Mater. Chem.* **2002**, *12*, 2430–2432. [CrossRef]
38. Yu, H.; Liu, Y.; Brock, S.L. Synthesis of discrete and dispersible MoS_2 nanocrystals. *Inorg. Chem.* **2008**, *47*, 1428–1434. [CrossRef] [PubMed]
39. Kogovšek, J.; Kalin, M. Various MoS_2-, WS_2- and C-based micro- and nanoparticles in boundary lubrication. *Tribol. Lett.* **2014**, *53*, 585–597. [CrossRef]
40. Pamies, R.; Espejo, C.; Carrión, F.J.; Morina, A.; Neville, A.; Bermúdez, M.D. Rheological behavior of multiwalled carbon nanotube-imidazolium tosylate ionic liquid dispersions. *J. Rheol.* **2017**, *61*, 279–289. [CrossRef]
41. Grigoriev, A.Y.; Kavaliova, I.N.; Kreivaitis, R.; Kupchinskas, A.; Padgurskas, Y. Effect of fatty-acid composition and structure of alkyl radicals of plant oil triglycerides on their tribotechnical characteristics. *J. Frict. Wear* **2016**, *37*, 552–555. [CrossRef]
42. Díez-Pascual, A.M.; Díez-Vicente, A.L. Development of linseed oil–TiO_2 green nanocomposites as antimicrobial coatings. *J. Mater. Chem. B* **2015**, *3*, 4458–4471. [CrossRef]
43. Bexell, U.; Olsson, M.; Johansson, M.; Samuelsson, J.; Sundell, P.-E. A tribological study of a novel pre-treatment with linseed oil bonded to mercaptosilane treated aluminium. *Surf. Coat. Technol.* **2003**, *166*, 141–152. [CrossRef]
44. Kalin, M.; Kogovšek, J.; Remškar, M. Mechanisms and improvements in the friction and wear behavior using MoS_2 nanotubes as potential oil additives. *Wear* **2012**, *280–281*, 36–45. [CrossRef]
45. Tomala, A.; Ripoll, M.R.; Gabler, C.; Remškar, M.; Kalin, M. Interactions between MoS_2 nanotubes and conventional additives in model oils. *Tribol. Int.* **2017**, *110*, 140–150. [CrossRef]
46. Paskvale, S.; Remškar, M.; Čekada, M. Tribological performance of TiN, TiAlN and CrN hard coatings lubricated by MoS_2 nanotubes in Polyalphaolefin oil. *Wear* **2016**, *352–353*, 72–78. [CrossRef]